Original Article
Exploration and validation of m7G-related genes as signatures in the immune microenvironment and prognostic indicators in low-grade glioma

Wen Zhen[1,3], Xueshi Shan[1], Xiangdong Cui[2], Pengxiang Ji[1], Ping Zhang[1], Minghua Wang[3*], Zhan Cai[1*]

[1]Department of Neurosurgery, Suzhou Ruihua Orthopedic Hospital, Suzhou 215104, Jiangsu, China; [2]School of Marine Science and Technology, Northwestern Polytechnical University, Xi'an 710072, Shaanxi, China; [3]Department of Biochemistry and Molecular Biology, Medical College, Soochow University, Suzhou 215123, Jiangsu, China. *Equal contributors.

Abstract: Objectives: Currently, an increasing number of studies are focusing on the impact of m7G modification in cancer. This study aims to investigate the prognostic value of m7G-related genes in low-grade glioma (LGG). Methods: LGG samples were obtained from the CGGA database, and normal samples were obtained from GTEx. Differentially expressed m7G-related genes were identified, and genes highly associated with macrophage M2 in LGG patients were identified by immuno-infiltration and WGCNA analysis. The intersection of differentially expressed m7G-related genes and macrophage M2-associated genes yielded candidate genes, and hub genes were identified using 5 algorithms in CytoHubba. Enrichment analysis verified the relevant pathways of hub genes, and their performance in tumor classification was evaluated. Results: A total of 3329 differentially expressed m7G-related genes were identified. 1289 genes were highly associated with macrophage M2 in LGG patients. The intersection of m7G-related genes and results in WGCNA yielded 840 candidate genes, and six hub genes (STXBP1, CPLX1, PAB3A, APBA1, RIMS1, and GRIN2B) were identified. Hub genes were enriched in synaptic transmission-related pathways and showed good performance for tumor classification. There were significant differences in survival levels between clusters. Conclusions: The identified m7G-related genes may provide new insight into the treatment and prognosis of LGG.

Keywords: Low-grade glioma (LGG), N7-methylguanosine, immune microenvironment, WGCNA, prognostic signature

Introduction

Glioma is a group of tumors arising from glial cells in the central nervous system and is the most common type of brain tumor. The World Health Organization (WHO) classifies gliomas into four grades based on their histopathologic features, genetic alterations, and clinical behavior [1]. Low-grade glioma (LGG) is WHO grade II, III gliomas that are less aggressive and have a better prognosis compared to high-grade gliomas (HGG). However, LGG still causes severe neurological deficits and affects the quality of life of patients. Second, the infiltrative growth pattern of LGG leads to its frequent recurrence and increases the difficulty of complete surgical resection [2].

The factors that contribute to the development and progression of LGG are complex. Several genetic alterations associated with LGG have been identified, such as mutations and copy number alterations in genes such as IDH1/2, TP53 and ATRX. These genes play a key role in altering cellular metabolism, DNA repair and chromatin remodeling, affecting tumor progression [3, 4]. Recent evidence suggests that epigenetic modifications such as RNA methylation and histone modifications also play a crucial role in the pathogenesis of LGG. m7G is an important RNA modification that is achieved by attaching guanine molecules with methylation at the 5' end of RNA. This modification is present at the end of most eukaryotic mRNAs and has many important functions. It includes initi-

ating transcriptional processes, enhancing translation efficiency and stabilizing RNA molecules [5]. Several studies have shown that abnormal levels of m7G modifications are associated with the formation and progression of a variety of tumors. For example, the m7G regulator METTLE is an oncogenic factor in bladder cancer. METTLE mediates the translation of EFEMP1 by altering the m7G modification of tRNA and inhibiting ribosomal pausing during tRNA-mRNA codon recognition. Promoting tumorigenesis [6]. In hepatocellular carcinoma, METTL1 promotes tumor proliferation and metastasis by inhibiting PTEN-related signaling pathways [7]. Another m7G regulator, WDR4, contributes to the poor prognosis of esophageal squamous cell carcinoma by decreasing the transcriptional level of ULK1, a negative regulator in autophagy-related pathways [6]. In addition, m7G modifications are involved in the regulation of tumor cell stemness and drug resistance [8]. Therefore, investigating the specific mechanism of action of m7G modification in LGG may provide important information for the diagnosis and prognosis of this cancer.

The immune tumor microenvironment (TME) refers to the environment surrounding the tumor consisting of multiple components including immune cells, extracellular mechanisms and cytokines. Immune cells play an important role in the TME as they fight against tumor expansion and recognize and destroy cancer cells. At the same time, cancer cells can secrete some cytokines or control immune cell functions, rendering immune cells useless or shifting to a tumor-supportive state, thus evading immune attack and promoting tumor progression [9]. Several studies have shown that immune cell infiltration in TME is associated with m7G modification. For example, a study on human hepatocellular carcinoma found significantly reduced levels of m7G modification in tumor tissues and significant changes in the expression of genes associated with antitumor immune response. Further studies found that the reduction in m7G modification may lead to a decrease in the number and activity of hepatic natural killer cells in the tumor microenvironment, thus affecting the anti-tumor effects of immune cells [10]. In addition, another study found that changes in the level of m7G modification altered the expression of certain key genes in T cells, thus affecting T cell expansion and activity in TME [11]. However, the mechanism of m7G modification in immune infiltration is not clear, especially in LGG. Therefore, clarifying the characteristics of m7G-related gene-mediated immune infiltration may help improve the survival prognosis of LGG patients.

This study was based on CGGA and GTEx databases. The differential analysis identified m7G regulators that were differentially expressed in LGG, and further Pearson correlation analysis screened for differential genes associated with m7G. Techniques such as CIBERSORT and WGCNA were applied to screen candidate genes in LGG that were associated with m7G and involved in immune infiltration. Enrichment analysis of the candidate genes was performed to detect the biological processes they are involved in, and protein interaction networks were constructed. 6 hub genes were finally identified, and tumor classification validated their value in LGG and evaluated in the TCGA dataset. The results showed that these hub genes could be used as signatures for optimizing LGG prognosis.

Materials and methods

Data source and preprocessing

The tumor sample data in this study were obtained from the CGGA database (Home|CGGA - Chinese Glioma Genome Atlas) (DataSet ID: mRNAseq_325), and we downloaded the FPKM values. The dataset included 325 glioma samples. 137 LGG samples were screened based on the primary tumor, tumor classification as WHO II and III (LGG), complete information on sample survival, and survival days >30 days. Normal cortex samples from the GTEx project were obtained from the UCSC (UCSC Xena) in 105 cases as controls. It is worth noting that the data downloaded from CGGA were the raw FPKM values, while the data in UCSC were log2 (fpkm+0.001) processed. Therefore, we first performed an fpkm^2-0.001 calculation for the expression in the normal group. Then we merged the tumor group and normal group data sets, and the "normalizeBetweenArrays" function in the "limma" package was used to eliminate the batch effect between the two groups. The log2 (fpkm+1) was calculated for the expressions in the combined dataset for normalization purposes. This resulted in the

experimental matrix used for our subsequent analysis. Data for the test set were obtained from TCGA (GDC (cancer.gov)) by doing the same screening as the experimental set, yielding 481 LGG samples. 37 m7G regulators were obtained from the GSEA database.

Identification of differentially expressed genes and differential m7G regulators in LGG

The "limma" package in R was applied to obtain differentially expressed genes (DEGs) between LGG and normal samples in the expression data. The significance analysis was performed and the selection criteria were |log2FC| >0.5 and adjusted p value <0.05. There were some differentially expressed m7G regulators in the DEGs.

Identification of M7G-related genes

Pearson correlation analysis was performed to investigate the relationship between DEGs and differential m7G regulators. Specifically, DEGs that exhibited Pearson correlation coefficients greater than 0.7 and p values less than 0.05 were considered as m7G-related genes.

Immune cell infiltration assessment

CIBERSORT is an immune cell analysis tool based on gene expression data that allows the quantification of multiple immune cell types and their relative percentages in tissue samples. CIBERSORT uses a linear regression model that compares the gene expression profile of a sample with known reference gene expression profiles of different immune cell subpopulations and calculates the relative abundance of different immune cell subpopulations in the sample [12]. To identify differences in immune cell composition between LGG and normal groups, all genes in the matrix were analyzed with CIBERSORT. We used LM22 signature and 1000 replacements in R to obtain the proportion of each type of immune cell in the two groups of samples and kept the immune cells that showed a different distribution between the two groups of samples for subsequent analysis.

Weighted gene co-expression network analysis

WGCNA (Weighted Gene Co-expression Network Analysis) is a systems biology approach for gene expression data analysis that can be used to construct gene co-expression networks, identify key gene modules and central genes associated with biological processes and diseases, and explore their role in cellular function, disease development, and progression [13]. Genes in the top 50% of the absolute median deviation in the expression matrix were selected and analyzed using the "WGCNA" package in R. WGCNA was applied to the co-expression network based on Pearson correlation coefficient matrix. To satisfy the scale-free topology, an appropriate soft threshold of β is determined. Then the genes are clustered into functional modules of different colors and clustered and classified using a minimized dynamic tree-cutting algorithm. The module size is set to 100 and the minimum merge height is 0.4. Gray modules denote genes that cannot be merged. Module signature genes (MEs) indicate the expression profiles of corresponding genes in different modules. The level of differentially distributed immune cell infiltration was selected as a clinical trait. Module affiliation (MM) indicates the correlation of MEs with gene expression. Gene significance (GS) was defined as the Spearman correlation coefficient of gene expression with clinical traits. Modules with the highest GS were considered as critical modules and genes with |MM| >0.8, |GS| >0.5 were identified as key genes [14].

Enrichment analysis of candidate genes

First, the intersecting genes from m7G-related genes and key genes in WGCNA were taken as candidate genes. GO enrichment analysis classified gene function into three aspects: molecular function (MF), cellular component (CC), and biological process (BP). In KEGG enrichment analysis, target gene sets were mapped to pathway information in the KEGG database to identify metabolic pathways and signaling pathways that may play important roles in the research question [15]. We used Metascape (Metascape) to perform the enrichment analysis.

Construction of protein interaction network to identify hub genes

The protein interaction network of candidate genes was generated in the String database (string-db.org), and the interaction score thresh-

old was set to 0.7. The results were imported into Cytoscape, and to ensure the accuracy of hub gene identification, we used five algorithms in CytoHubba with reference to previous studies [16]. The final hub genes were obtained by taking the intersection of the top 25 genes of each algorithm.

Consensus clustering analysis

To further explore the biological characteristics of the hub gene, 137 patients were clustered into different subtypes based on the expression of the hub gene using the "Consensus-ClusterPlus" package in R. To verify the stability of the subtypes, 500 replicates were performed with *p*-Item equal to 0.8. The optimal *k* value (*k*=3) was determined to obtain stable clustering. Principal component analysis (PCA) was used to examine the clustering results. Differences in survival and hub gene expression were also compared between the different clusters. ImmuneScore, StromalScore, ESTIM-ATEScore and TumorPurity were determined between different clusters using the ESTIMATE algorithm. ssGSEA determined the scores of 28 immune cells.

Validation of hub gene features

We retrieved datasets related to low-grade glioma in the TCGA database and screened 481 LGG samples based on the primary tumor, tumor classification as WHO II or III (LGG), complete information on sample survival, and survival days >30 days. Log2 (fpkm+1) processing was done on the expression matrix. Consensus clustering analysis was done according to hub gene to examine the function of hub gene in identifying tumor subtypes and clinical prognosis. The clustering results were examined by PCA and survival analysis. In addition, we downloaded immunohistochemical images from the publicly available Human Protein Atlas (http://www.proteinatlas.org) for comparison of protein expression levels associated with gene features.

Statistical analysis

All data analyses were conducted using R version 4.2.1. Details of the specific bioinformatic analyses performed can be found in the respective subsections. Statistical significance was defined as a *p* value less than 0.05.

Results

Differentially expressed genes in LGG

By comparing LGG samples with normal brain tissue samples, 4174 differentially expressed genes were obtained (2000 up-regulated genes and 2174 down-regulated genes; see **Figure 1A**). 9 out of 37 m7G regulators were differentially expressed. The box line plot (**Figure 1B**) and heat map (**Figure 1C**) results showed that these 9 m7G regulators were significantly different between LGG and normal samples. Among them, 7 genes were up-regulated and 2 genes were down-regulated. The positions of these 9 m7G regulators on the chromosomes are shown in **Figure 1D**.

Immune cell infiltration analysis

Applying the CIBERSORT algorithm, we investigated the differences in immune infiltration between LGG and normal samples in 22 immune cell subpopulations (**Figure 2A**). As shown in the violin plot (**Figure 2B**), T cells follicular helper ($P<0.001$), Macrophages M0 ($P<0.001$), Macrophages M2 ($P<0.001$), and Dendritic cells resting ($P<0.001$) were different compared to normal samples. Dendritic cells activated ($P<0.001$) and Mast cells activated ($P<0.001$) were more infiltrated in LGG. Conversely, B cells memory ($P<0.001$), Plasma cells ($P<0.001$), T cells regulatory ($P=0.001$), NK cells resting ($P<0.001$), Macrophages M1 ($P<0.001$), Mast cells resting ($P<0.001$), Eosinophils ($P<0.001$), and Neutrophils ($P<0.001$) infiltrated significantly less than normal samples in LGG.

Construction of co-expression network

We selected the genes in the top 50% of the median absolute deviation in the expression matrix for WGCNA screening. To detect possible outlier samples, a clustering tree including 137 samples and infiltrate-associated immune cells was built by applying the average linkage method. The results showed no abnormal samples were identified (**Figure 3A**). Then, we built a scale-free co-expression network with scale-free R^2=0.9 and soft threshold power β=5 (**Figure 3B**). The clustering height was set to 0.4 to merge the highly correlated modules (**Figure 3C**). The results of the initial and merged modules are shown under the clustering tree (**Figure 3D**).
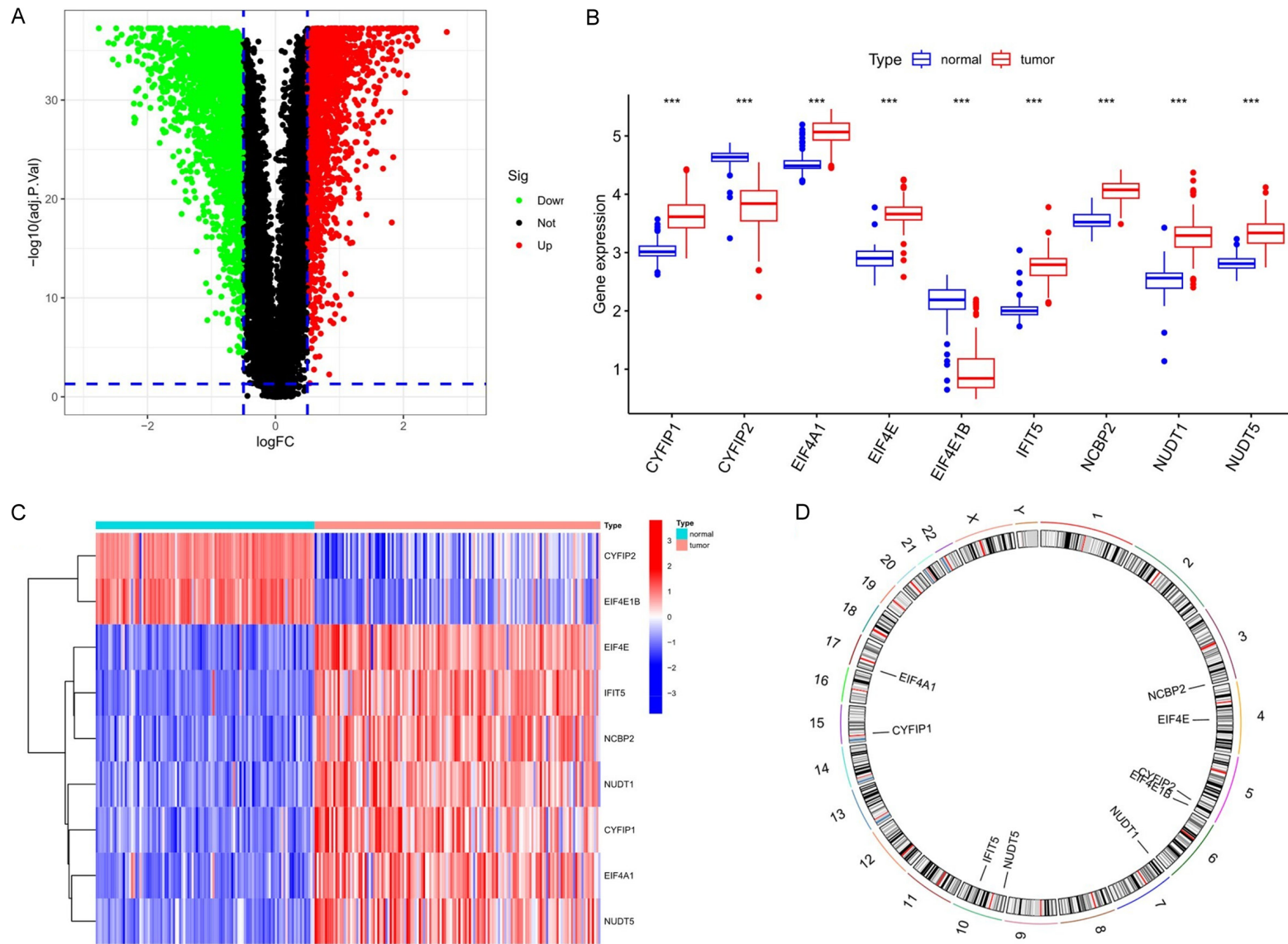
Figure 1. Differentially expressed genes in LGG. A. Volcano plot showing DEGs between LGG and normal samples. Red dots represent upregulated genes in LGG, green dots represent downregulated genes, and black dots represent genes with no significant change. B. Boxplot showing the differential expression of 9 m7G regulators in LGG and normal samples. The Wilcoxon test was used to compare differences. *P<0.05; **P<0.01; ***P<0.001. C. Heatmap displaying the expression pattern of m7G regulators in LGG and normal samples. D. Chromosome locations and names of the 9 differentially expressed m7G regulators.

Figure 2. Analysis of immune cell infiltration. A. The relative proportions of 22 types of infiltrated immune cells in LGG and normal samples are shown. B. A violin plot displays the significant changes in immune cell infiltration levels between LGG and normal samples.
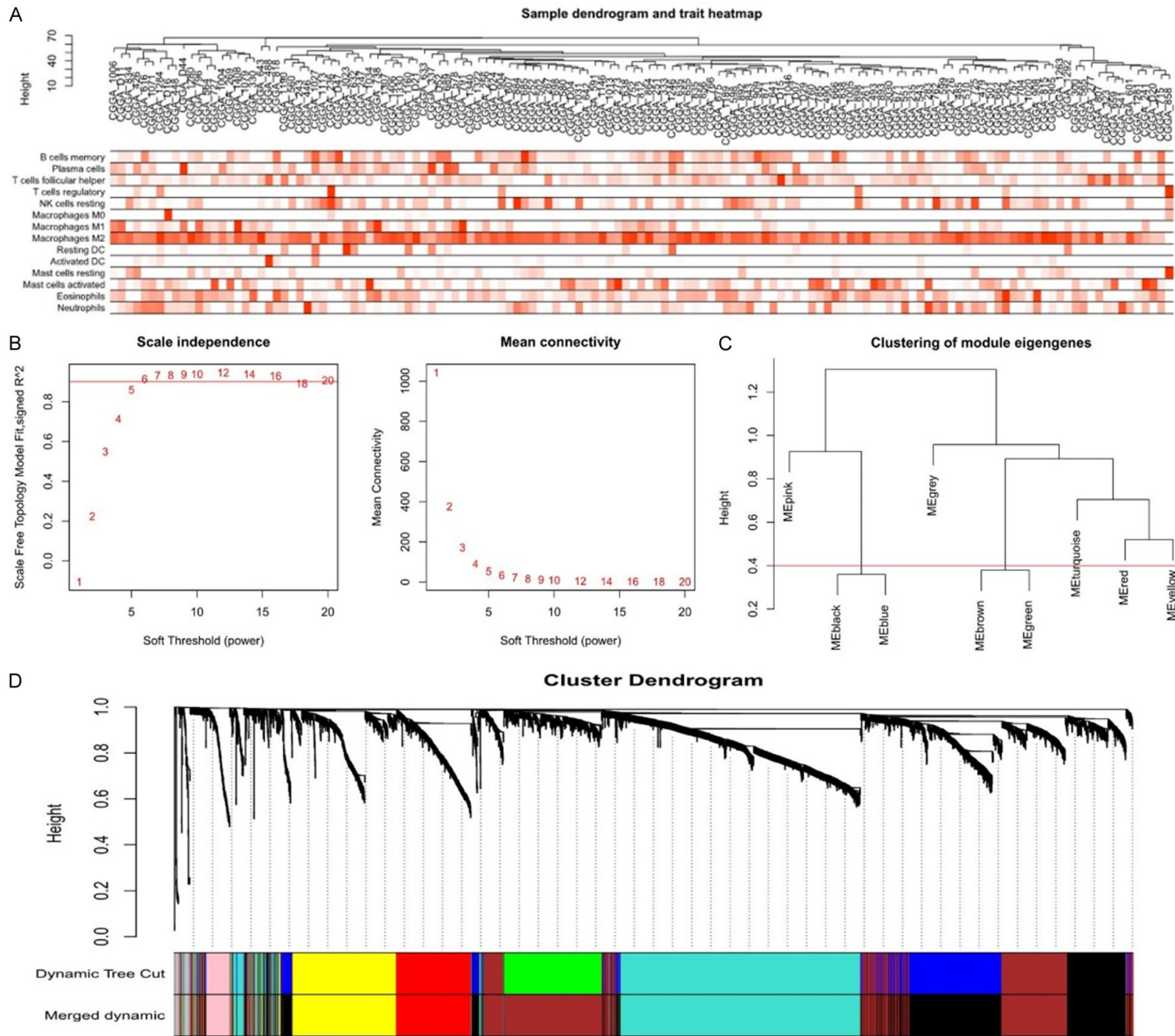
Figure 3. Construction of a co-expression network. A. The LGG samples were clustered based on their expression levels, and the color intensity indicates the infiltration level of immune cells. B. The appropriate soft-power value for the graphs of scale independence, mean connectivity, and scale-free topology was found to be 5. C. To identify and combine similar modules, clustering dendrograms were cut at a height of 0.4. D. The original and merged modules are displayed beneath the clustering tree.

Identification of WGCNA key modules

The relationship between modules and infiltrating immune cells was explored by calculating the correlation between ME values and clinical features. We identified seven co-expression modules, and gray modules were considered as unassignable gene collections. The results showed a positive correlation between the turquoise module and T cells follicular helper (r=0.39, P=2e-06) and a negative correlation with Macrophages M2 (r=-0.44, P=9e-08), and a negative correlation between the black module and T cells follicular helper (r=-0.39, P=3e-06), and a negative correlation with Macrophages M1 (r=0.43, P=2e-07). Based on the ME values, we identified turquoise as the most clinically significant module (**Figure 4A**). In addition, we plotted GS scatter plots of T cells follicular helper and Macrophages M2 versus MM in turquoise (**Figure 4B**, **4C**). The results showed that the turquoise module was highly correlated with immune infiltration. We further selected 1289 genes from the turquoise module for subsequent analysis based on the criteria of |MM| >0.8 and |GS| >0.5.

Acquisition of candidate genes

In the differential analysis we obtained 9 differentially expressed m7G regulators. 3329 m7G-related DEGs were identified by Pearson correlation analysis (**Figure 5A**). The 840 candidate genes were obtained by taking the intersection of m7G related DEGs and genes in the turquoise module (**Figure 5B**).

Identification of hub genes and enrichment analysis

After constructing the PPI network of candidate genes in String, the results were collated in Cytoscape. We used five algorithms of CytoHubba, including MCC, DMNC, MNC, Degree and EPC, and took the intersection of the top 25 genes in each algorithm to get the final 6 hub genes (**Figure 6A**). They were STXBP1, CPLX1, RAB3A, APBA1, RIMS1, and GRIN2B. Hub genes were mainly enriched in Dopamine

Neurotransmitter Release Cycle, Transmission across Chemical Synapses, Neurexins, and Neuroligins pathways (**Figure 6B**).

Identification of tumor subtypes

Based on six hub genes, 137 tumor samples were clustered by CDF and delta area (**Figure 7A**, **7B**). When k=3, three clusters were found, namely cluster 1, cluster 2 and cluster 3 (**Figure 7C**). PCA analysis verified that samples from the three subgroups were clustered separately, confirming the reliability of the clustering results (**Figure 7D**). KM survival analysis showed that patients in cluster 3 performed better than the other two groups (P=3e-07) in **Figure 7E**. Based on clustering, we combined other clinical manifestations to represent the expression differences of the six pivotal genes in the form of heat maps (**Figure 8A**). The results showed that the expression of the six pivotal genes was significantly higher in cluster 3 than in cluster 1, suggesting that these pivotal genes may be markers for identifying different tumor clusters. In addition, the heat map shows the differences between the different clusters based on the ESTIMATE algorithm, ImmuneScore, StromalScore and EstimateScore mentioned in the methods section (**Figure 8B**). Previous studies have shown that patients with high purity in a wide range of tumors usually have better survival (Li et al., 2022b). This is consistent with the results of our study. Tumor purity was higher in group 3 and most immune cells had more infiltration in group 1, which had poorer survival.

Validation of hub genes

To validate the ability of the hub gene in LGG prognosis. Tumor subtype analysis was performed for 481 samples of TCGA. Delta area and CDF clustering showed (**Figure 9A**, **9B**) that the division into 3 clusters was reasonable (**Figure 9C**). PCA and survival analysis also confirmed the reliability of clustering results (**Figure 9D**, **9E**). These results indicated that the ability of hub gene in LGG prognosis is worthy of affir-
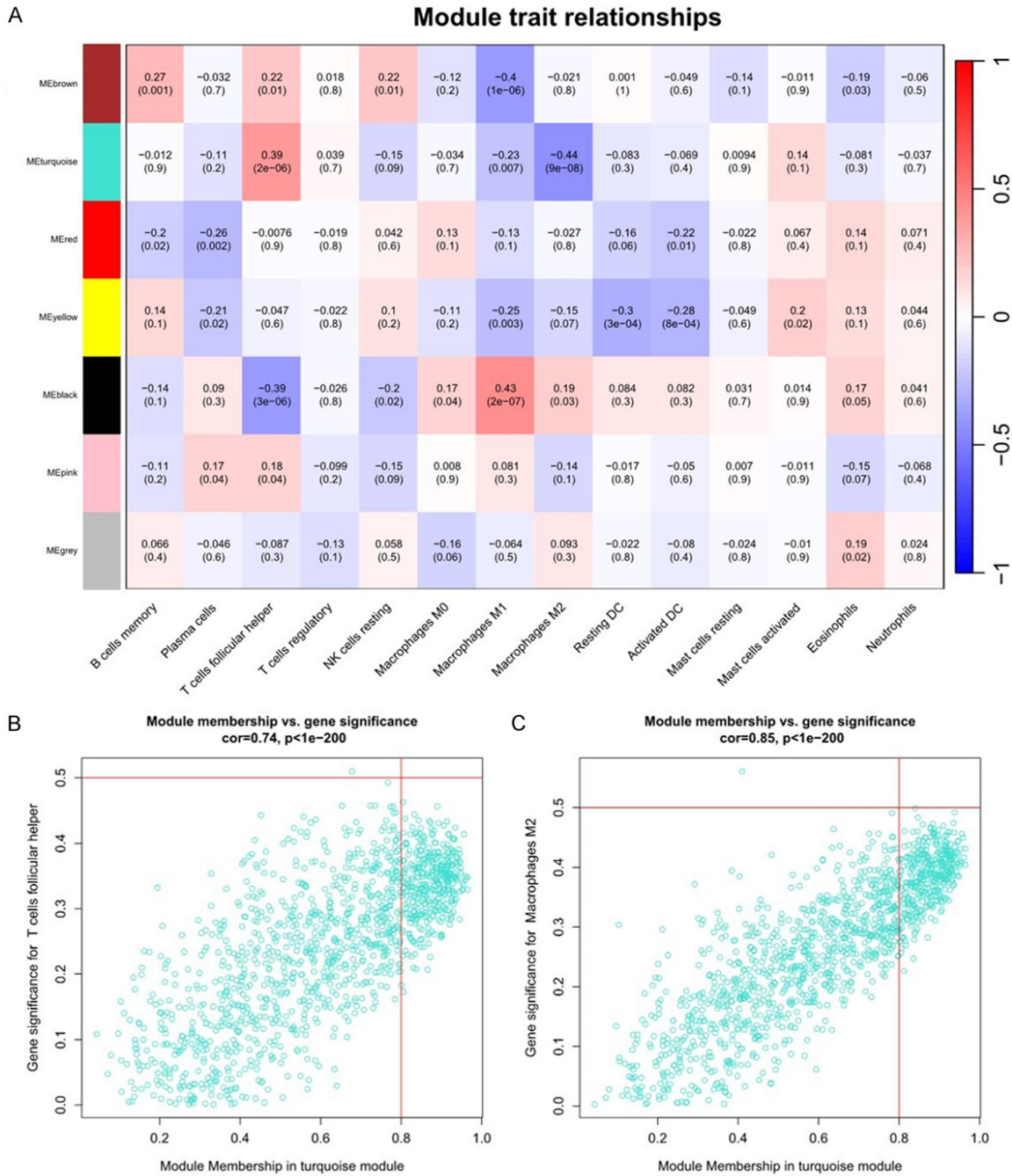
Figure 4. Screening of clinically related modules. (A) A heatmap presents the module-trait correlation, with red indicating a positive correlation and blue indicating a negative correlation. Gene significance for LGG across all modules was calculated, and the turquoise module was determined to be the clinically related module. (B, C) Scatter plots display the correlation between module membership (MM) and gene significance (GS), with revised MM and GS values. (B) T cells follicular helper, and (C) Macrophages M2 are shown.

mation. Finally, to determine the clinical relevance of these six hub gene expressions, we analyzed the protein expressions encoded by these six genes using clinical samples from HPA. Compared to their expression levels in normal samples, STXBP1, CPLX1, and RAB3A showed HIGH staining in normal samples (**Figure 10A**, **10C** and **10E**) and low expression in LGG (**Figure 10B**, **10D** and **10F**), RIMS1 and GRIN2B were not detected in cancer tissue sections, and APBA1 had no corresponding information in the website.
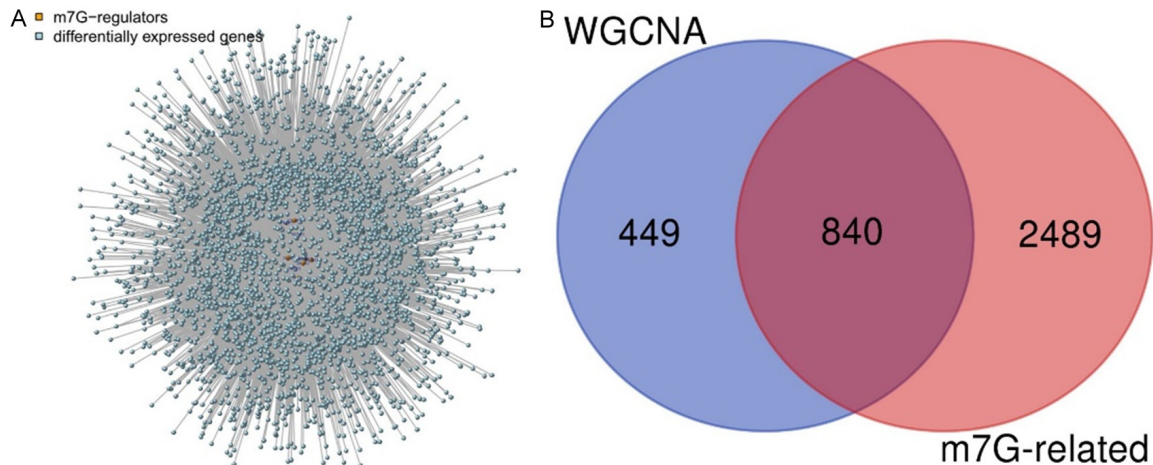
Figure 5. Acquisition of candidate hub genes. A. Screening of m7G related genes. The orange dots represent the m7G regulators, the green dots represent the m7G regulated genes, and the lines represent the correlations between the dots. B. Venn diagram of m7G-related genes and the genes of the turquoise modules in WGCNA. Intersection indicates candidate hub genes.

Discussion

Low-grade glioma is a group of relatively slow-growing, relatively less malignant glial tumors. It usually has a good prognosis and long-term survival rate. However, LGG is usually located in important areas of the brain, such as motor, language, and visual areas, and therefore surgical resection or tumor enlargement may lead to neurological dysfunction. Secondly, low-grade glioma also has the risk of transforming into high-grade glioma. Therefore, early diagnosis and screening, as well as prognosis after diagnosis, are crucial to reduce the risk from LGG. The factors associated with the development and progression of LGG are complex and vary greatly between patients, making it difficult to identify consistent predictors or biomarkers. To be able to provide some new theories for the treatment and prognosis of LGG, in this study, we used the CGGA database of glioma-related datasets. 9 m7G regulators were identified by differential expression gene analysis, and m7G-related genes were explored. Applying the CIBERSORT algorithm to analyze the infiltration of immune cells, WGCNA identified the most significant modules with macrophage M2. Among the modules, 840 m7G-related candidate genes were screened. Candidate genes were used to construct a PPI network and the final six hub genes (STXBP1, CPLX1, RAB3A, APBA1, RIMS1 and GRIN2B) were identified by five algorithms in CytoHubba. These hub genes were mainly enriched in the Dopamine

Neurotransmitter Release Cycle, Transmission across Chemical Synapses, Neurexins and neuroligins pathways. These genes have some value in tumor clusters and show significantly different survival levels between clusters. We found evidence in the RMVar database (RMVar-Database of functional variants involved in RNA modification (renlab.org)) that supports the m7G modification of our hub genes. We defined the above genes as hub genes involved in macrophage M2 m7G modification in LGG patients. This may provide us with some insights into LGG prognosis.

Macrophages are a class of immune cells that play an important role in the tumor immune microenvironment. Macrophages are usually differentiated into two types, M1 and M2. Macrophage M1 cells are mainly involved in immune response processes with bactericidal and antitumor effects [17]. Previous studies mentioned that in gliomas, macrophage M2 stimulates glioma blood vessel formation and growth through the release of growth factors such as VEGF, and promotes tumor cell migration and invasion through interactions [18]. In addition, macrophage M2 regulates immune responses in the TME by suppressing T cell activation and proliferation, thereby limiting tumor antigen presentation and recognition and promoting the immune escape of tumors [19]. In our study, we found a significant increase in the number of macrophages M2 and a relative decrease in macrophages M1 in
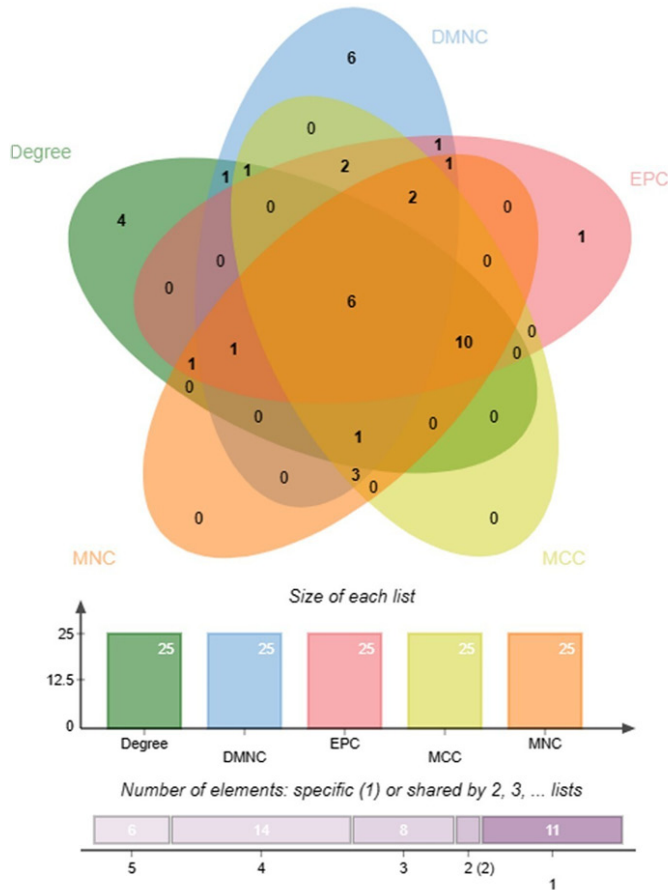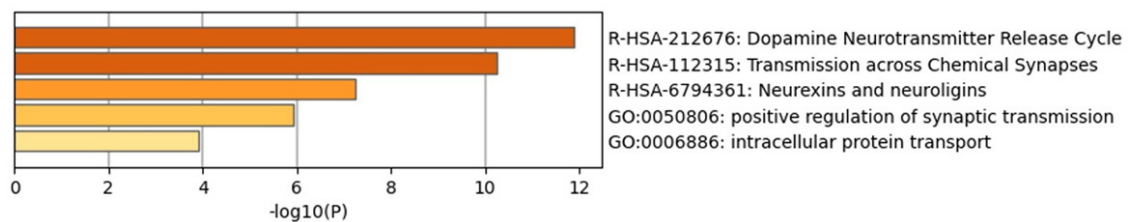
Figure 6. Identification of hub genes and enrichment analysis. A. A Venn diagram between five algorithms of Cyto-Hubba to identify hub genes in LGG. B. Functional enrichment analysis of hub genes.

tumor samples. This imbalance may promote tumor growth and spread. We observed that these 6 hub genes are lowly expressed in LGG, and their expression trends are consistent across different clusters. Samples in the clusters with higher expression levels have higher survival rates, while samples in the clusters with lower expression levels have relatively lower survival rates. There are differences in ImmuneScore, ESTIMATEScore, and Stromal-Score among different clusters. Specifically, ImmuneScore, ESTIMATEScore, and Stromal-Score are significantly higher in the group with lower hub gene expression levels than in the group with higher expression levels. M2 macro-

phages infiltrate more in cluster 1, which has a lower survival rate. Therefore, we believe that the silencing of hub genes leads to the proliferation of M2 macrophages, indirectly promoting the occurrence and development of tumors. Currently, there are therapeutic strategies targeting the inhibition of M2 macrophage function, intervention in its signaling pathway, and immunotherapy. Thus, the hub genes we identified can serve as new targets for effective treatment of tumors.

Looking from another perspective, we found that these hub genes are enriched in synaptic transmission-related pathways. Synaptic trans-
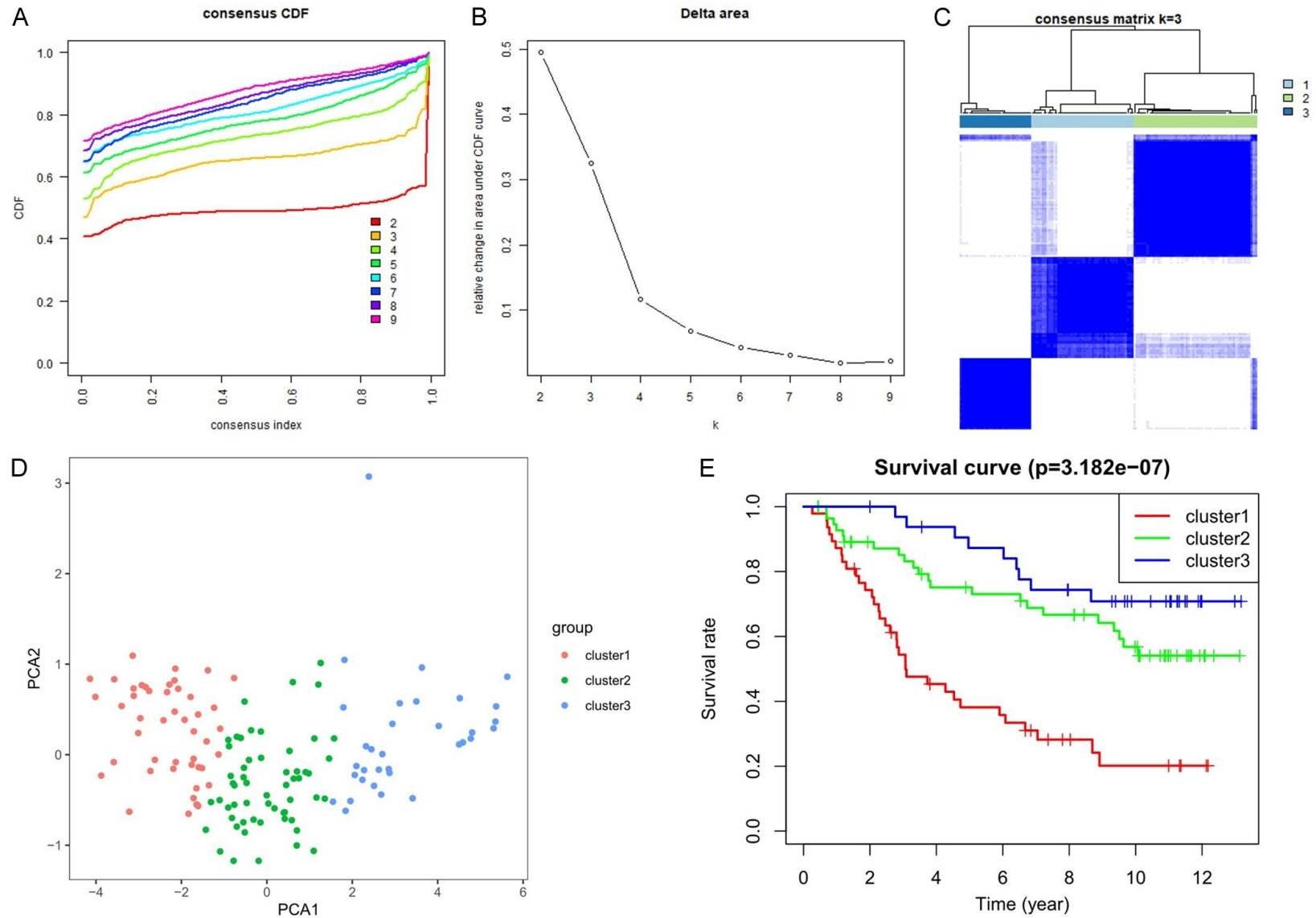
Figure 7. Consistent cluster analysis in the experimental set. A. Cumulative distribution function (CDF) for consistent clustering with *k* values ranging from 2-9. B. Relative changes in the area under the CDF curve for *k* values ranging from 2-9. C. Consensus clustering matrix using *k*=3. D. Principal component analysis showed effective clustering. E. Comparison of Kaplan-Meier overall survival (OS) rates among the three clusters (*P*=3e-07).
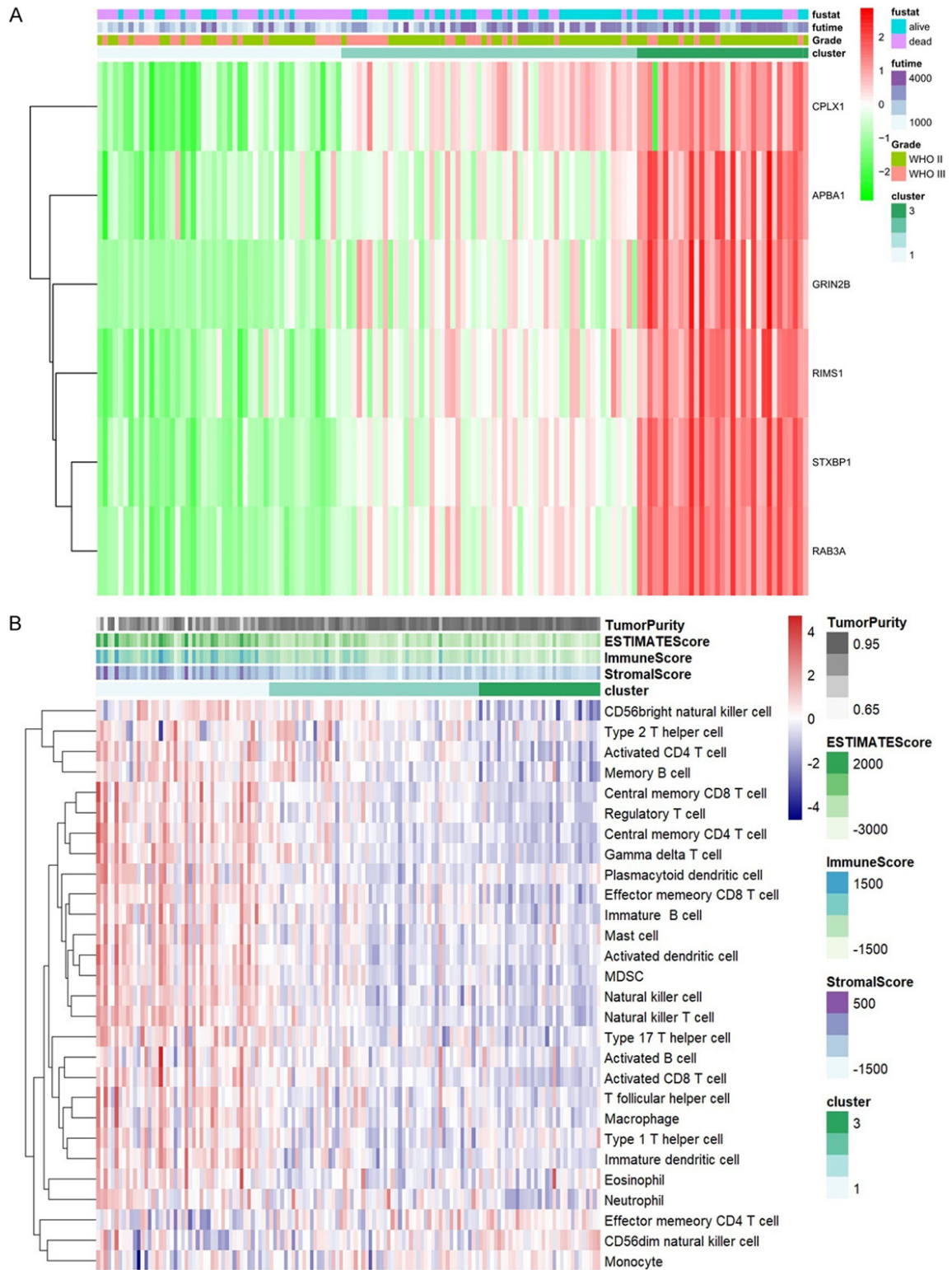
Figure 8. Consensus clustering of hub genes and clinicopathologic characteristics. A. Heatmap displaying the expression pattern of hub genes across three identified clusters (red, high expression level; green, low expression level). Clinicopathologic characteristics of each cluster are also presented. B. Comparison of immune score, stromal score, ESTIMATE score, and tumor purity between the three identified clusters.
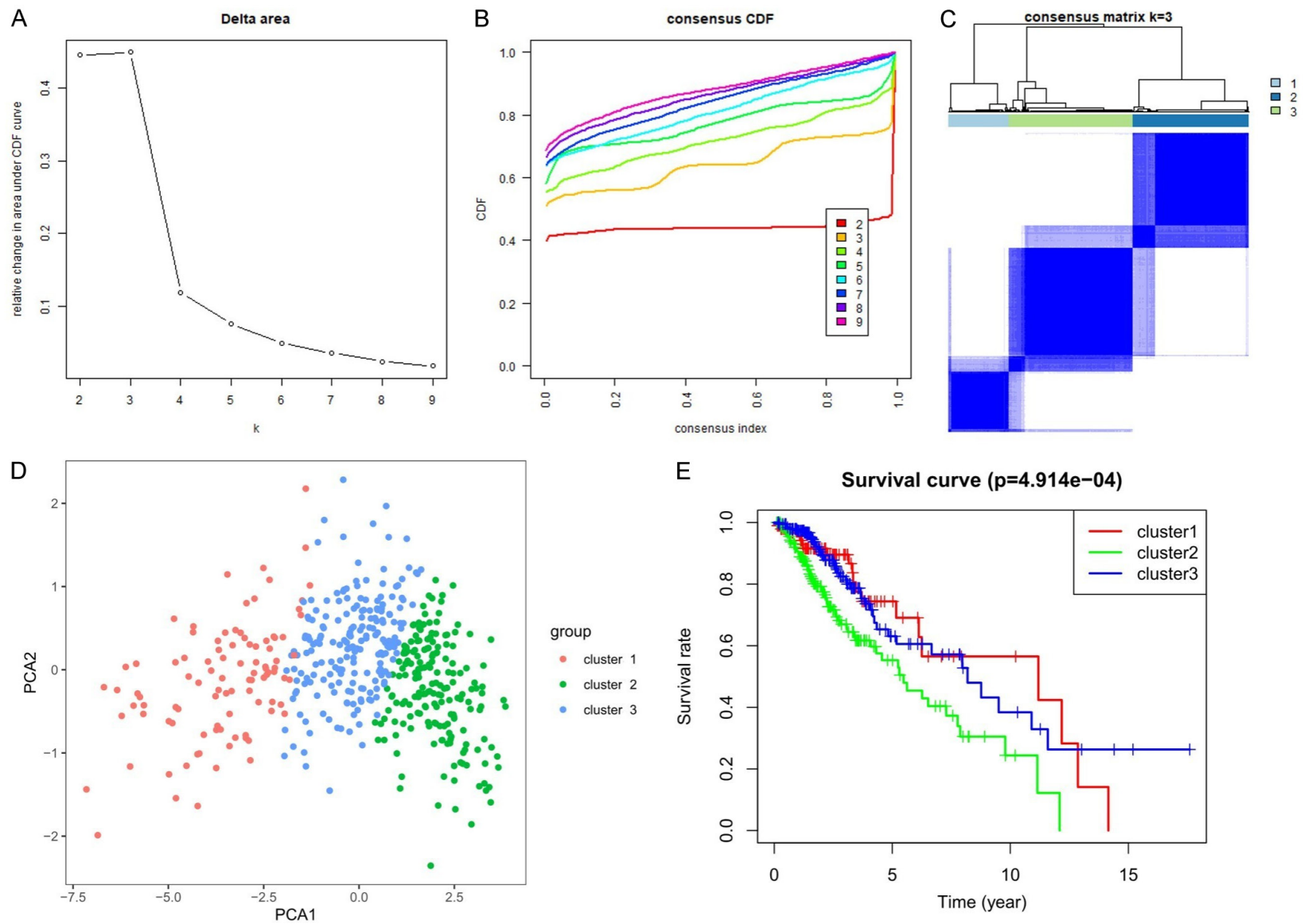
Figure 9. Consistent clustering analysis in the test set. A. Relative change in the area under the cumulative distribution function (CDF) curve for *k*=2-9. B. CDF plot showing consistent clustering at *k*=2-9. C. Consensus clustering matrix obtained with *k*=3. D. Principal component analysis confirming the effectiveness of the clustering approach. E. Kaplan-Meier overall survival curves for the three identified clusters, demonstrating significant differences in OS rates (P=4e-04).
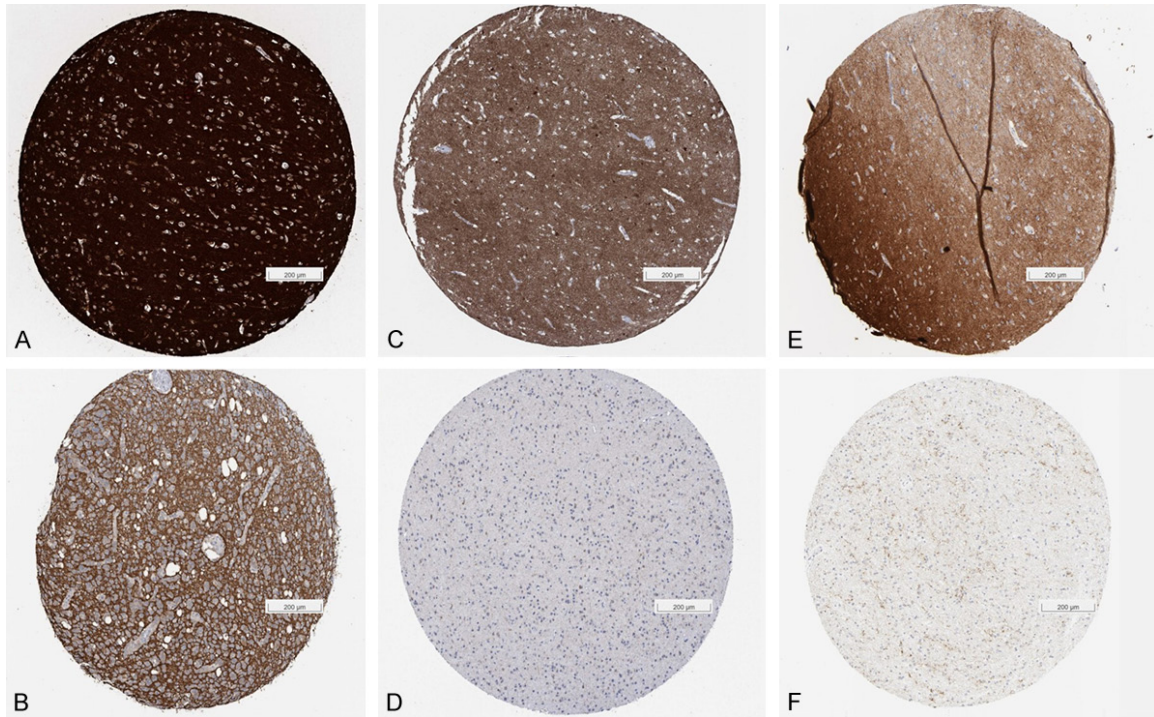
Figure 10. Human protein Atlas immunohistochemistry using anti-STXBP1, anti-CPLX1, and anti-RAB3A antibodies. Normal brain (A, C, E) vs. low-grade glioma (B, D, F). The staining in normal samples is stronger than that in the tumor.

mission is an important mode of information transfer between neurons and between neurons and target cells. Many tumor cells have neuron-like characteristics, such as membrane potential and calcium ion concentration, so they can also synthesize, store, and release neurotransmitters and affect surrounding tissues through synaptic transmission. Second, some key molecules, pathways, and mechanisms in synaptic transmission are also involved in the proliferation, invasion, and metastasis of tumor cells [20, 21]. STXBP1 is a protein involved in cellular secretion. Mutations in STXBP1 lead to impaired stability of synaptic proteins, resulting in a range of brain disorders such as developmental delay, mental retardation, and epilepsy [22, 23]. Furthermore, STXBP1 is involved in regulating the activity of NRF1, a class of transcription factors with high activity in cancer. downregulation of STXBP1 in gliomas predicts the degree of malignancy in those with high NRF1 activity [24]. This is consistent with our findings that STXBP1 is downregulated in LGG. APBA1, a member of the amyloid β preprotein binding family, was found to be lowly expressed in Ewing sarcoma [25]. In addition, APBA1 and STXBP1 were found to

have the ability to collaborate in insulin release. A calmodulin, CASTK, enhances the collaboration of APBA1 with STXBP1 and affects vesicular transport during insulin release [26]. RIMS1 is a protein involved in the presynaptic response of neurons and has an important role in neurotransmitter release. The high expression of RIMS1 in gastric cancer was negatively correlated with patient survival. In addition, RIMS1 expression was found to be downregulated in adamantinomatous craniopharyngioma [27]. The function of RAB3A is similar to that of RIMS1. RIMS1 and RAB3A are required to interact during terminal vesicle transport and affect synaptic transport function. Abnormal neurotransmitter transmission may be a contributing factor to hippocampal lesions [28]. GRIN2B is one of the NMDA-type glutamate receptor subunits that regulate biological processes such as calcium ion concentration, synaptic plasticity, and neural signaling [29]. GRIN2B is associated with many neurodevelopmental disorders, such as epilepsy, developmental delay, and language impairment [30]. There is also some evidence that GRIN2B is significantly more mutated in stage III lung cancer than in stage I patients [31]. CPLX1 has been identified

as a biomarker for gastric cancer, and high expression of CPLX promotes proliferation, motility, and invasion of gastric cancer cells. and is associated with a poorer prognosis [32]. In addition, CPLX is a synapse-encoded protein and its deletion was detected in a mouse model of Alzheimer's disease [33]. In-depth exploration of the mechanisms of synaptic transmission in tumors and the search for possible targets and therapeutic strategies are expected to provide new ideas and approaches for the treatment of tumors. The results of tumor clustering showed that these hub genes can effectively stratify LGG into different subtypes. Further exploration of the synaptic transmission mechanism in tumors may help us understand the occurrence, growth patterns, and metastasis rules of different types of LGG. The search for possible targets and treatment strategies is expected to provide new ideas and methods for the treatment of LGG.

Our study has some limitations. Our data and clinical survival studies are based on the CGGA database only. Careful consideration is needed in extending our findings to patients of different races. In addition, it is necessary to experimentally validate the specific m7G modification mechanism of these genes in LGG in subsequent studies. Finally, the functions and molecular mechanisms of these genes are complex and need to be further validated by cellular and animal experiments.

Conclusion

Our study identifies the role of m7G-related genes in LGG. Using multiple biological methods, STXBP1, CPLX1, PAB3A, APBA1, RIMS1, and GRIN2B were identified as protective prognostic factors against macrophage M2 infiltration in LGG. The results of these genes in the prognostic survival of patients with different types of LGG support our conclusions. Perspectives on regulating synaptic transmission and macrophage M2 have provided new insight into immunotherapy for LGG.

Acknowledgements

Disclosure of conflict of interest

None.

Address correspondence to: Zhan Cai, Department of Neurosurgery, Suzhou Ruihua Orthopedic Hospital, Suzhou 215104, Jiangsu, China. E-mail: pxca@sina.com; Minghua Wang, Department of Biochemistry and Molecular Biology, Medical College, Soochow University, Suzhou 215123, Jiangsu, China. E-mail: mhwang@suda.edu.cn

References

[1] Louis DN, Perry A, Reifenberger G, von Deimling A, Figarella-Branger D, Cavenee WK, Ohgaki H, Wiestler OD, Kleihues P and Ellison DW. The 2016 World Health Organization classification of tumors of the central nervous system: a summary. Acta Neuropathol 2016; 131: 803-820.

[2] Lim M, Xia Y, Bettegowda C and Weller M. Current state of immunotherapy for glioblastoma. Nat Rev Clin Oncol 2018; 15: 422-442.

[3] Yan H, Parsons DW, Jin G, McLendon R, Rasheed BA, Yuan W, Kos I, Batinic-Haberle I, Jones S, Riggins GJ, Friedman H, Friedman A, Reardon D, Herndon J, Kinzler KW, Velculescu VE, Vogelstein B and Bigner DD. IDH1 and IDH2 mutations in gliomas. N Engl J Med 2009; 360: 765-773.

[4] Cancer Genome Atlas Research Network; Brat DJ, Verhaak RG, Aldape KD, Yung WK, Salama SR, Cooper LA, Rheinbay E, Miller CR, Vitucci M, Morozova O, Robertson AG, Noushmehr H, Laird PW, Cherniack AD, Akbani R, Huse JT, Ciriello G, Poisson LM, Barnholtz-Sloan JS, Berger MS, Brennan C, Colen RR, Colman H, Flanders AE, Giannini C, Grifford M, Iavarone A, Jain R, Joseph I, Kim J, Kasaian K, Mikkelsen T, Murray BA, O'Neill BP, Pachter L, Parsons DW, Sougnez C, Sulman EP, Vandenberg SR, Van Meir EG, von Deimling A, Zhang H, Crain D, Lau K, Mallery D, Morris S, Paulauskis J, Penny R, Shelton T, Sherman M, Yena P, Black A, Bowen J, Dicostanzo K, Gastier-Foster J, Leraas KM, Lichtenberg TM, Pierson CR, Ramirez NC, Taylor C, Weaver S, Wise L, Zmuda E, Davidsen T, Demchok JA, Eley G, Ferguson ML, Hutter CM, Mills Shaw KR, Ozenberger BA, Sheth M, Sofia HJ, Tarnuzzer R, Wang Z, Yang L, Zenklusen JC, Ayala B, Baboud J, Chudamani S, Jensen MA, Liu J, Pihl T, Raman R, Wan Y, Wu Y, Ally A, Au-

man JT, Balasundaram M, Balu S, Baylin SB, Beroukhim R, Bootwalla MS, Bowlby R, Bristow CA, Brooks D, Butterfield Y, Carlsen R, Carter S, Chin L, Chu A, Chuah E, Cibulskis K, Clarke A, Coetzee SG, Dhalla N, Fennell T, Fisher S, Gabriel S, Getz G, Gibbs R, Guin R, Hadjipanayis A, Hayes DN, Hinoue T, Hoadley K, Holt RA, Hoyle AP, Jefferys SR, Jones S, Jones CD, Kucherlapati R, Lai PH, Lander E, Lee S, Lichtenstein L, Ma Y, Maglinte DT, Mahadeshwar HS, Marra MA, Mayo M, Meng S, Meyerson ML, Mieczkowski PA, Moore RA, Mose LE, Mungall AJ, Pantazi A, Parfenov M, Park PJ, Parker JS, Perou CM, Protopopov A, Ren X, Roach J, Sabedot TS, Schein J, Schumacher SE, Seidman JG, Seth S, Shen H, Simons JV, Sipahimalani P, Soloway MG, Song X, Sun H, Tabak B, Tam A, Tan D, Tang J, Thiessen N, Triche T Jr, Van Den Berg DJ, Veluvolu U, Waring S, Weisenberger DJ, Wilkerson MD, Wong T, Wu J, Xi L, Xu AW, Yang L, Zack TI, Zhang J, Aksoy BA, Arachchi H, Benz C, Bernard B, Carlin D, Cho J, DiCara D, Frazer S, Fuller GN, Gao J, Gehlenborg N, Haussler D, Heiman DI, Iype L, Jacobsen A, Ju Z, Katzman S, Kim H, Knijnenburg T, Kreisberg RB, Lawrence MS, Lee W, Leinonen K, Lin P, Ling S, Liu W, Liu Y, Liu Y, Lu Y, Mills G, Ng S, Noble MS, Paull E, Rao A, Reynolds S, Saksena G, Sanborn Z, Sander C, Schultz N, Senbabaoglu Y, Shen R, Shmulevich I, Sinha R, Stuart J, Sumer SO, Sun Y, Tasman N, Taylor BS, Voet D, Weinhold N, Weinstein JN, Yang D, Yoshihara K, Zheng S, Zhang W, Zou L, Abel T, Sadeghi S, Cohen ML, Eschbacher J, Hattab EM, Raghunathan A, Schniederjan MJ, Aziz D, Barnett G, Barrett W, Bigner DD, Boice L, Brewer C, Calatozzolo C, Campos B, Carlotti CG Jr, Chan TA, Cuppini L, Curley E, Cuzzubbo S, Devine K, DiMeco F, Duell R, Elder JB, Fehrenbach A, Finocchiaro G, Friedman W, Fulop J, Gardner J, Hermes B, Herold-Mende C, Jungk C, Kendler A, Lehman NL, Lipp E, Liu O, Mandt R, McGraw M, McLendon R, McPherson C, Neder L, Nguyen P, Noss A, Nunziata R, Ostrom QT, Palmer C, Perin A, Pollo B, Potapov A, Potapova O, Rathmell WK, Rotin D, Scarpace L, Schilero C, Senecal K, Shimmel K, Shurkhay V, Sifri S, Singh R, Sloan AE, Smolenski K, Staugaitis SM, Steele R, Thorne L, Tirapelli DP, Unterberg A, Vallurupalli M, Wang Y, Warnick R, Williams F, Wolinsky Y, Bell S, Rosenberg M, Stewart C, Huang F, Grimsby JL, Radenbaugh AJ and Zhang J. Comprehensive, integrative genomic analysis of diffuse lower-grade gliomas. N Engl J Med 2015; 372: 2481-2498.

[5] Furuichi Y. Discovery of m(7)G-cap in eukaryotic mRNAs. Proc Jpn Acad Ser B Phys Biol Sci 2015; 91: 394-409.

[6] Luo Y, Yao Y, Wu P, Zi X, Sun N and He J. The potential role of N(7)-methylguanosine (m7G) in cancer. J Hematol Oncol 2022; 15: 63.

[7] Tian QH, Zhang MF, Zeng JS, Luo RG, Wen Y, Chen J, Gan LG and Xiong JP. METTL1 overexpression is correlated with poor prognosis and promotes hepatocellular carcinoma via PTEN. J Mol Med (Berl) 2019; 97: 1535-1545.

[8] Huang M, Long J, Yao Z, Zhao Y, Zhao Y, Liao J, Lei K, Xiao H, Dai Z, Peng S, Lin S, Xu L and Kuang M. METTL1-mediated m7G tRNA modification promotes lenvatinib resistance in hepatocellular carcinoma. Cancer Res 2023; 83: 89-102.

[9] Lv B, Wang Y, Ma D, Cheng W, Liu J, Yong T, Chen H and Wang C. Immunotherapy: reshape the tumor immune microenvironment. Front Immunol 2022; 13: 844142.

[10] Liu P, Dong C, Shi H, Yan Z, Zhang J and Liu J. Constructing and validating of m7G-related genes prognostic signature for hepatocellular carcinoma and immune infiltration: potential biomarkers for predicting the overall survival. J Gastrointest Oncol 2022; 13: 3169-3182.

[11] Liu Y, Jiang B, Lin C, Zhu W, Chen D, Sheng Y, Lou Z, Ji Z, Wu C and Wu M. m7G-related gene NUDT4 as a novel biomarker promoting cancer cell proliferation in lung adenocarcinoma. Front Oncol 2023; 12: 1055605.

[12] Newman AM, Liu CL, Green MR, Gentles AJ, Feng W, Xu Y, Hoang CD, Diehn M and Alizadeh AA. Robust enumeration of cell subsets from tissue expression profiles. Nat Methods 2015; 12: 453-7.

[13] Langfelder P and Horvath S. WGCNA: an R package for weighted correlation network analysis. BMC Bioinformatics 2008; 9: 559.

[14] Kong Y, Feng ZC, Zhang YL, Liu XF, Ma Y, Zhao ZM, Huang B, Chen AJ, Zhang D, Thorsen F, Wang J, Yang N and Li XG. Identification of immune-related genes contributing to the development of glioblastoma using weighted gene co-expression network analysis. Front Immunol 2020; 11: 1281.

[15] Kanehisa M, Furumichi M, Tanabe M, Sato Y and Morishima K. KEGG: new perspectives on genomes, pathways, diseases and drugs. Nucleic Acids Res 2017; 45: D353-D361.

[16] Li Q, Gao X, Luo X, Wu Q, He J, Liu Y, Xue Y, Wu S and Rao F. Identification of hub genes associated with immune infiltration in cardioembolic stroke by whole blood transcriptome analysis. Dis Markers 2022; 2022: 8086991.

[17] Najafi M, Hashemi Goradel N, Farhood B, Salehi E, Nashtaei MS, Khanlarkhani N, Khezri Z, Majidpoor J, Abouzaripour M, Habibi M, Kashani IR and Mortezaee K. Macrophage polarity in cancer: a review. J Cell Biochem 2019; 120: 2756-2765.

[18] Zhang G, Tao X, Ji B and Gong J. Hypoxia-driven M2-polarized macrophages facilitate cancer aggressiveness and temozolomide resistance in glioblastoma. Oxid Med Cell Longev 2022; 2022: 1614336.

[19] Yamaguchi Y, Gibson J, Ou K, Lopez LS, Ng RH, Leggett N, Jonsson VD, Zarif JC, Lee PP, Wang X, Martinez C, Dorff TB, Forman SJ and Priceman SJ. PD-L1 blockade restores CAR T cell activity through IFN-gamma-regulation of CD163+ M2 macrophages. J Immunother Cancer 2022; 10: e004400.

[20] Monje M. Synaptic communication in brain cancer. Cancer Res 2020; 80: 2979-2982.

[21] Fels E, Muniz-Castrillo S, Vogrig A, Joubert B, Honnorat J and Pascual O. Role of LGI1 protein in synaptic transmission: from physiology to pathology. Neurobiol Dis 2021; 160: 105537.

[22] Abramov D, Guiberson NGL and Burre J. STXBP1 encephalopathies: clinical spectrum, disease mechanisms, and therapeutic strategies. J Neurochem 2021; 157: 165-178.

[23] Lammertse HCA, van Berkel AA, Iacomino M, Toonen RF, Striano P, Gambardella A, Verhage M and Zara F. Homozygous STXBP1 variant causes encephalopathy and gain-of-function in synaptic transmission. Brain 2020; 143: 441-451.

[24] Bhawe K, Felty Q, Yoo C, Ehtesham NZ, Hasnain SE, Singh VP, Mohapatra I and Roy D. Nuclear respiratory factor 1 (NRF1) transcriptional activity-driven gene signature association with severity of astrocytoma and poor prognosis of glioblastoma. Mol Neurobiol 2020; 57: 3827-3845.

[25] Roundhill EA, Chicon-Bosch M, Jeys L, Parry M, Rankin KS, Droop A and Burchill SA. RNA sequencing and functional studies of patient-derived cells reveal that neurexin-1 and regulators of this pathway are associated with poor outcomes in Ewing sarcoma. Cell Oncol (Dordr) 2021; 44: 1065-1085.

[26] Zhang K, Wang T, Liu X, Yuan Q, Xiao T, Yuan X, Zhang Y, Yuan L and Wang Y. CASK, APBA1, and STXBP1 collaborate during insulin secretion. Mol Cell Endocrinol 2021; 520: 111076.

[27] Yang J, Hou Z, Wang C, Wang H and Zhang H. Gene expression profiles reveal key genes for early diagnosis and treatment of adamantinomatous craniopharyngioma. Cancer Gene Ther 2018; 25: 227-239.

[28] Suo Z, Yang J, Zhou B, Qu Y, Xu W, Li M, Xiao T, Zheng H and Ni C. Whole-transcriptome sequencing identifies neuroinflammation, metabolism and blood-brain barrier related processes in the hippocampus of aged mice during perioperative period. CNS Neurosci Ther 2022; 28: 1576-1595.

[29] Bell S, Maussion G, Jefri M, Peng H, Theroux JF, Silveira H, Soubannier V, Wu H, Hu P, Galat E, Torres-Platas SG, Boudreau-Pinsonneault C, O'Leary LA, Galat V, Turecki G, Durcan TM, Fon EA, Mechawar N and Ernst C. Disruption of GRIN2B impairs differentiation in human neurons. Stem Cell Reports 2018; 11: 183-196.

[30] Myers SJ, Yuan H, Kang JQ, Tan FCK, Traynelis SF and Low CM. Distinct roles of GRIN2A and GRIN2B variants in neurological conditions. F1000Res 2019; 8: F1000 Faculty Rev-1940.

[31] Liu Y, Duan J, Zhang F, Liu F, Luo X, Shi Y and Lei Y. Mutational and transcriptional characterization establishes prognostic models for resectable lung squamous cell carcinoma. Cancer Manag Res 2023; 15: 147-163.

[32] Li Y, Leng Y, Dong Y, Song Y, Wu Q, Jiang N, Dong H, Chen F, Luo Q and Cheng C. Cyclin B1 expression as an independent prognostic factor for lung adenocarcinoma and its potential pathways. Oncol Lett 2022; 24: 441.

[33] Jesko H, Wieczorek I, Wencel PL, Gassowska-Dobrowolska M, Lukiw WJ and Strosznajder RP. Age-related transcriptional deregulation of genes coding synaptic proteins in Alzheimer's disease murine model: potential neuroprotective effect of fingolimod. Front Mol Neurosci 2021; 14: 660104.